CHAPTER II

Structural and Optical Properties of core-shell Ag_2S-HgS nanostructurs

Semiconductor nanomaterials are of keen research interest now a days because of their novel electrical and optical properties. Several works have been attempted to make semiconductor nanocrystals which can possess profound applicability in the field of optoelectronics as well as environmental cleaning. But among those semiconductors, Ag_2S or other sulfide materials studied very merely in comparison to the emphasis that has bestowed upon TiO_2 nanoparticles. But TiO_2 has a limitation due to its band gap 3.25 eV which makes it applicable only in the UV regime without any additional element while Ag_2S has a bulk band gap of 1.1 eV indicating they can be used in the IR regime. So, we started this work with questions whose answers to be unveiled as we go down this chapter

- Can we tune the optical properties of Ag_2S nanoparticles by coating it with another sulfide material namely HgS? Can it be extended from UV to IR regime i.e the whole solar regime?

- Reports are published on TYPE 1 core-shell nanostructures which are useful for LEDs and Lasing purpose whilst TYPE 2 are potential source for photovltaics as well as photocatalysis. Can we see in a single core-shell semiconductor, properties of TYPE 1 and TYPE 2 s which can be achieved just by changing the shell parameters?

In this chapter, we have discussed about synthesis of a novel material core-shell Ag_2S-HgS where a lower band gap material i.e. Ag_2S (1.1 eV) is coated with a higher band gap material HgS (2.1 eV). Detailed study is reported on the structural, morphological and optical characteristic of the sample. We have shown that with increase in shell thickness, there is a transition from TYPE 1 to TYPE 2 core-shell structure in the sample.

Among the semiconductor nanoparticles, silver sulfide systems have good scopes in photoelectric and thermoelectric applications [1].Several reports have been published regarding fabrication and application of Ag_2S nanostructures [2-5]. Again, coating a nanomaterial (typically lower energy gap) by another material (typically higher energy gap) yields core-shell nanostructures where the cores and shells may be any kind of colloidal particles, i.e. metals, insulators and all classes of semiconductors [6].

Generally, the core material having a certain band gap is capped by a material with a larger band gap where the conduction band energy of the capping material is higher (more negative in an electrochemical sense) than that of the core material and the valence band energy of the capping material being lower (more positive on the electrochemical scale) than that of the core material. This type of core-shell structure is called TYPE 1 core-shell structure. [6]. Due to this capping, the exciton photo generated in the core is prohibited from spreading over the entire particle and it is forced to recombine at the same time as spatially confined to the core. Mostly, an enhanced luminescence is observed as a result [6]. In TYPE 1 core-shell nanostructure, both electron and hole tend to confine themselves within the narrower band gap material. As a result, the emission energy is determined by band gap of of the core structure [7]. Again, the energy gradient present in case of TYPE 2 core-shell nano structure tends to spatially part the electron and the hole on each side of the core and shell. In this case, the emission energy is calculated by the energy difference between the conduction band edge of core structure and the valence band edge of shell structure, and hence, the band gap of TYPE 2 core-shell structure is lower than the band gap of either core or shell. In case of TYPE 1 core-shell nanostructures, the electron and hole experience a confinement potential that tends to localize both of them inside the core which reduces their interaction with surface traps and improves the emission quantum yields [8].

2.1 Materials for synthesis

Silver nitrate ($AgNO_3$), mercuric chloride ($HgCl_2$), Polyvinylpyrrolidon (PVP), carbon disulphide (CS_2) were obtained. For synthesis purposes ethanol and double distilled water were used.

2.1.1 Synthesis of Ag_2S nanoparticles

The Ag_2S nanoparticles were synthesized in a polymer host matrix. In a typical process [2], 0.3 g of $AgNO_3$ was dissolved in ethanol with vigorous stirring, and then 0.5 g of PVP was added into the solution and stirred for about 30 minutes. An excess amount of CS_2 was then introduced into the above solution and sulfuration reaction was allowed over 24 hours under no illumination. The black viscous solution was then

centrifuged to get the Ag_2S nanoparticles. The reaction mechanism involved in this process is as reported earlier [9]

2.1.2 Synthesis of core-shell Ag_2S-HgS nanoparticles

The core-shell nanoparticles were synthesized by adding $HgCl_2$ to the Ag_2S precursors so that Hg can react with S excessively and finally form Ag_2S-HgS structures. We prepared two solutions of $HgCl_2$ (0.1 M and 0.2 M) in water and each of these was added to the already prepared Ag_2S nanoparticles and stirred for 1 day.

Thus the formation of core-shell nanoparticles can easily be understood from the following equation [10]

$$mHgCl_2 + (Ag_2S)_n \longrightarrow (HgS)_m(Ag_2S)_{n-m} + 2mAgCl$$

Powder X-Ray diffraction (XRD) study of Ag_2S was performed by a Rigaku Miniflex X-Ray diffractometer with Cu K_α radiation (λ= 1.5418 Å) at 30 kV operating at with 2θ ranges from 10-70 degree.

The morphologies of synthesized nanoparticles were observed with a JEOL JEM 2100 Transmission electron microscope operating at an acceleration voltage of 200 KV. The samples were carefully prepared by dropping the material suspension (in ethanol) on the carbon coated copper grids. The EDX spectra were recorded with JEOL JSM SEM Model 6390 LV under liquid nitrogen environment.

The room temperature IR spectra of the core-shell particles were recorded in Nicolet Impact-410 IR spectrometer in KBR environment in the wavelength region 4000-450 cm^{-1}. The UV-Visible absorption spectra of the samples dispersed in Ethanol solvent were recorded in the range 200-700 nm using Shimadzu UV-2450 UV-Visible spectrophotometer. The photoluminescence spectra were recorded by a Perkinelemer Model LS 55 fluorescence spectrophotometer.

2.2 Results and discussion

The synthesized core Ag_2S and core-shell Ag_2S-HgS nanostructures are characterized with the tools mentioned in Materials and Method section and discussed as below.

2.2.1 XRD Characterization

X-ray diffraction is an important characterization tool for determination of phases, crystallite size as well as lattice strain. A collimated X-ray beam, generated by a cathode tube is focused to generate a monochromatic radiation that falls on the sample. The X-ray beam generates constructive interference which follows the Bragg's diffraction condition,

$$n\lambda=2dSin\theta \quad \ldots\ldots\ldots\ldots\ldots\ldots\ldots\ldots (2.1)$$

where λ is wavelength of X-ray radiation, n is the number of diffraction, d is the lattice spacing and θ is the diffraction angle [11]. X-ray diffraction provides the coherently diffracting grain size [12]. In case of bulk materials, a long range periodic atomic order is expected and the interaction of these materials with X-ray yields sharp Bragg diffraction peaks [13]. On the other hand, in nanocrystalline materials, a higher fraction of atoms are there on the amorphous grain boundary. Hence, instead of sharp peaks, the diffraction pattern of these materials shows broad peaks with diffused background. The broadening and diffuse background is due to the smaller crystallite size of the material and due to the presence of the amorphous grain boundary [14].

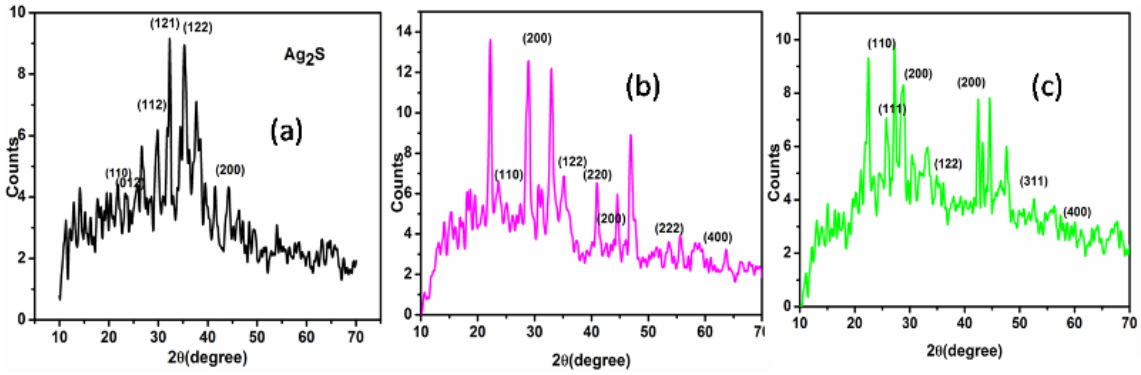

Fig. 2.1: XRD patterns of (a) core Ag_2S nanoparticles (b) core-shell Ag_2S-HgS (0.1 M Hg^{2+}) nanostructure and (c) core-shell Ag_2S-HgS (0.2 M Hg^{2+}) nanostructures.

Fig. 2.1 shows the XRD pattern of both core Ag_2S and core-shell Ag_2S-HgS nanostructures. Fig (a) shows the XRD of Ag_2S nanostructures where the peaks are namely around 2θ (degree) = 24.914(110), 26.321(012), 31.5 (112), 34.4 (121), 36.825 (122), 43.351 (200) correspond to that of monoclinic silver sulfide according to JCPDS file number 89-3840. In case of core-shell Ag_2S-HgS (0.1 M Hg^{2+})

nanostructure, [Fig. 2.1(b)] the peaks around 24.4, 36.8, 43.351 are also found which are also visible in the core-shell Ag_2S-HgS (0.2 M Hg^{2+}) [Fig. 2.1(c)] only the intensities are found to be enhanced with increasing shell thickness. Along with those peaks some additional peaks around 2θ(degree)= 31(200), 44(220), 54(222), 64(400) are prominent in the core-shell Ag_2S-HgS(0.1 M Hg^{2+}) structure and 26(111), 31(200), 44(220), 54(222), 64(400) which corresponds to HgS [15].

We have determined the lattice strain and crystallite size of each sample using Williamson-Hall (*W-H*) equation

$$\beta\cos\theta/\lambda = 0.9/D + 4€\sin\theta/\lambda \quad \text{.....(2.2)}$$

In eqn. (3.2), λ is the wavelength of X-ray, β and θ are the FWHM and diffraction angle of the diffraction peaks of Ag_2S nanostructure and both core-shells. *D* is the effective crystallite size considering lattice strain and € is the effective value of lattice strain.

Table 2.1: Calculation of lattice strain and crystallite size from W-H Plot

Sample	Crystallite size (nm)	Lattice strain
Ag_2S	10.2	-0.001665
Ag_2S/HgS (0.1 M Hg^{2+})	11.8	-0.00072
Ag_2S/HgS (0.2 M Hg^{2+})	12	-0.0035

From the table 2.1 it is precisely clear that the effective crystallite size of Ag_2S nanostructures gradually increases with addition of the shell. But a negative strain in observed in case of Ag_2S nanostructures. Negative strain indicates that the system is under external compressive forces and often lacks in grain boundary defects. Core-shell nanostructures are usually assumed to have the same band offsets as their bulk counterparts [16] and the red shifts of the absorption and photoluminescence peaks with increasing shell thickness are ascribed to a reduction in confinement associated with the presence of the shell, leading to a delocalization of electron wave functions from the core into the shell. Going down to fig. 2.8 and with the help of band gap calculations it is seen that a TYPE I band alignment prevails at the interface of Ag_2S

and HgS with the conduction band energy minimum and valence band energy maximum located in the Ag_2S domain. For a core with a larger radius R than the critical radius of delocalization of electron, overgrowth of a thin shell of HgS (0.1 M Hg^{2+}) imparts strong strain the shell, with little effect on the core material due to the large core size compared to the volume of the shell. This is experimentally proved as we can see from Table 2.1 that though negatively strained , still there is enhancement of lattice strain in core-shell Ag_2S-HgS (0.1 M Hg^{2+}). However, for this core size, when growth of a larger shell (0.2 M Hg^{2+}) exceeds the critical thickness, the electron can only be accommodated by the formation of defects that relax the strain between the two materials [17]. Therefore, the strain becomes more negative in case of core-shell Ag_2S-HgS (0.2 M Hg^{2+}) nanostructures.

2.2.2 TEM and EDX Characterization

XRD provides information of the crystallite size of a nanoparticle, while TEM offers the direct view of the size and shape of nanoparticles. Basically TEM instrument comprises of an electron gun which creates the electron beam, condenser lenses, a specimen stage that holds the sample and an imaging system containing some lenses that produces a magnified image or a diffraction pattern of the image on a screen [18]. The electrons wavelength is equal or less than the atomic dimension of the crystal and the highly energetic electrons can easily go through a solid letting information of the crystal which ordinary light microscope cannot give [18,19]. TEM is an important characterizing tool to realize the shape and size in the field of materials science, chemical science, biological science, etc.

Energy dispersive X-ray (EDX) analysis is a technique to find the composition of a material. It is used to measure the intensity of X-ray emission from a material as a function of the energy of the X-ray photons [20, 21]. When a sample is bombarded with high energy electron beam, the core electrons are excited to higher energy state thus leaving a hole in the lower energy core position. In this process X-rays are released which are characteristic of the element from which it is emitted. EDX instrument consists of an X-ray detector, a liquid nitrogen Dewar for cooling and software to collect and analyze the energy spectra [20-22]. The X-ray intensity provides information about the atomic fraction or mass fraction of each element

present in the material. This technique deals in the composition of almost all the elements in the periodic table, except H and He, since these two elements do not produce the characteristic X-rays [20]. EDX is a surface characterizing technique which gives information on elemental composition at the surface of a material not of the interior of a nanoparticle.

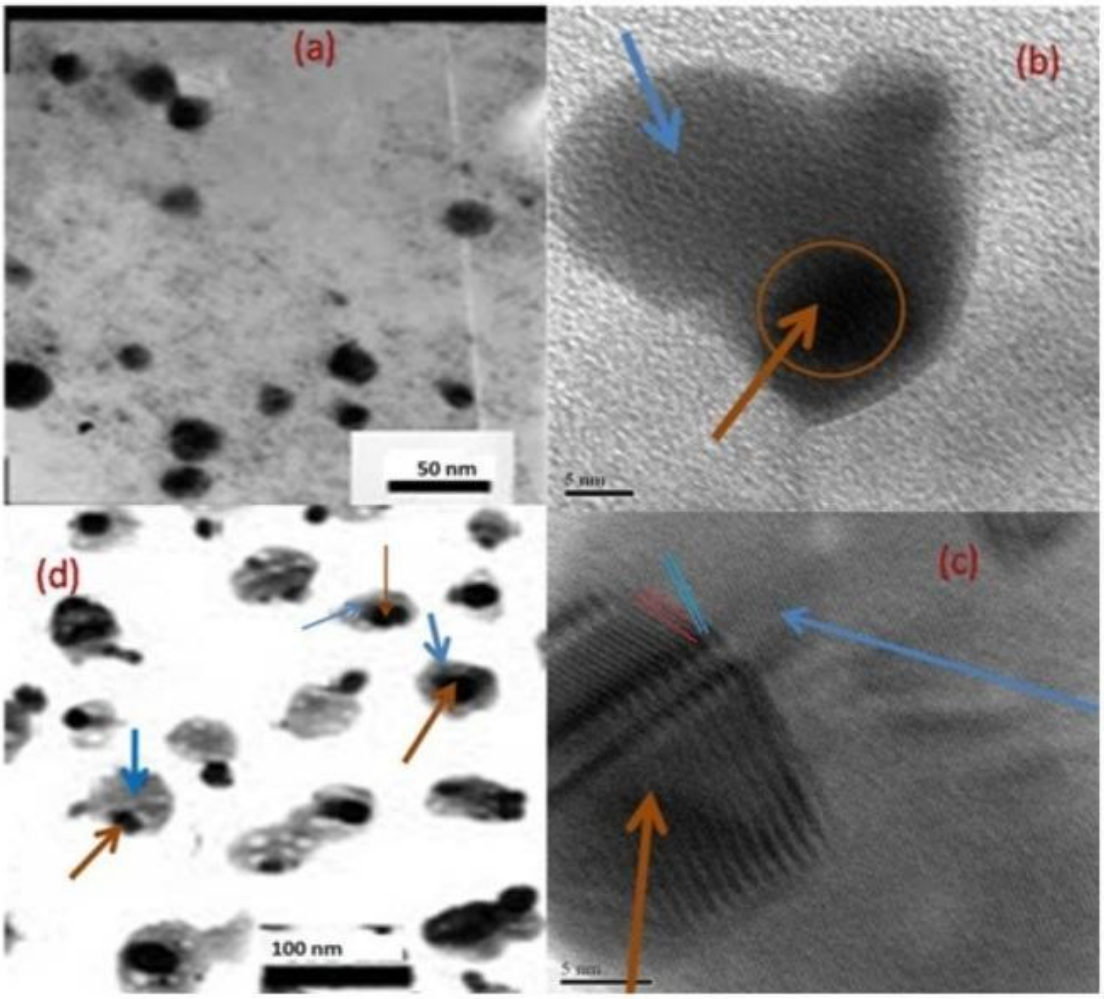

Fig. 2.2: TEM images (a) Ag_2S nanoparticles (b) Core-shell Ag_2S-HgS nanostructure (with 0.1 M Hg^{2+}) (c) HRTEM image of core-shell Ag_2S-HgS nanostructure (d) Core-shell Ag_2S-HgS nanostructure (with 0.2 M Hg^{2+})

Fig. 2.2 represents the TEM image of core Ag_2S nanostructures .The shape of the nanoparticles as seen in the fig are spherical with sizes varying from 15-30 nm. To compare the TEM images we prepared core-shell Ag_2S-HgS nanostructures with two

different shell thickness. We have used 0.1 M $HgCl_2$ solution (in water) for the first sample and 0.2 M $HgCl_2$ solution (in water) for the second sample. Fig (b) depicts the TEM image of a single core-shell Ag_2S-HgS (0.1 M $HgCl_2$) nanostructure of around 29 nm size and with a shell thickness of 10 nm where the core portion is indicated by dark brown arrows and the blue arrows indicate the surrounding lighter portion. Fig. (c) shows the HRTEM image of the core-shell nanostructure from where we can see two different orientations of lattice planes which are distinguished by brown arrow indicating core planes and blue arrow indicating the shell planes. From the HRTEM image, the lattice spacing is found as 6Å for the core particles and 2Å for the shell particles. Fig (d) represents the TEM image of core-shell structure (0.2 M $HgCl_2$) with particle sizes varying from 60-100 nm and also increase in shell thickness (starting from 31 nm) in most of the particles. Thus it is found that the shell thickness increased with increase in shell concentration in the sample.

Here, we have observed the non homogeneity of core-shell structures synthesized. As such they may be categorized as core-shell heterostructures.

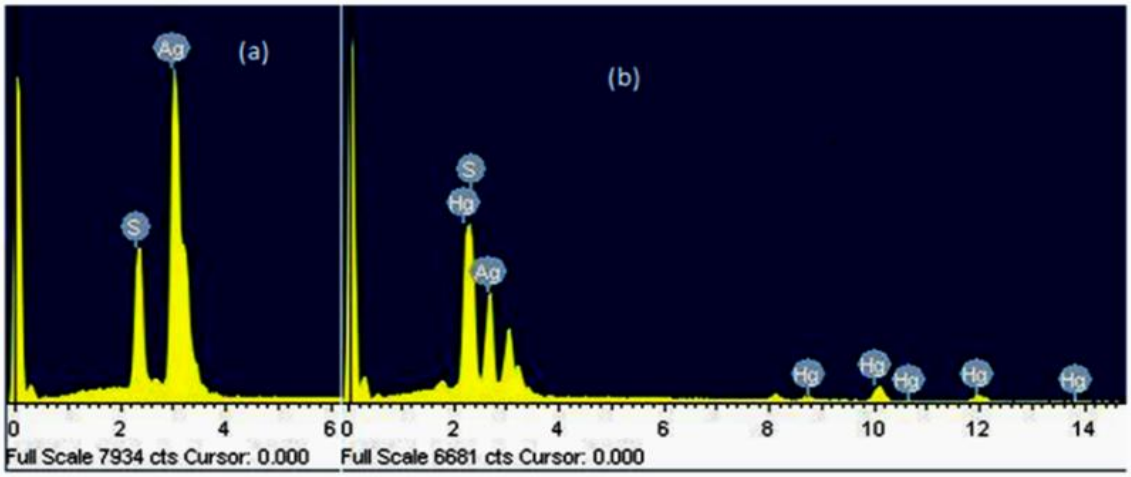

Fig. 2.3: EDX spectra (a) Ag_2S nanoparticles (b) Core-shell Ag_2S-HgS nanostructure

Fig. 2.3(a) and (b) shows the EDX pattern of core Ag_2S and core-shell Ag_2S-HgS nanostructures respectively. The EDX analysis clearly reveals the presence of all the consisting elements Ag, S and Hg.

2.2.3 FTIR Spectra analysis

In case of infrared (IR) spectroscopy, IR radiation is passed through a sample and during this process, a part of the radiations are absorbed by the sample and some of it is transmitted. The resulting spectrum represents the molecular absorption and transmission, generating a molecular fingerprint of the sample [30]. The sensitivity of IR instrument is too little to sense very small concentrations in the sub-ppm level. Spectral analysis is also tough since subtraction of background spectra had to be carried out manually [31]. Furthermore, conventional IR instruments are dispersive type which helps to distinguish between the individual frequencies generated by the source with prism or grating. On the contrary, an interferometer is used that creates signal containing entire frequencies and thus signal can be measured very fast [31]. In FTIR the IR radiation first passes through an interferometer that performs an optical inverse Fourier transform on the entering IR radiation. This IR beam interacts and is absorbed by the sample at different wavelengths. The intensity of the IR beam is detected by a detector which digitizes the signal and finally produces Fourier transformed image in the computer to get the IR spectrum of the sample gas [31].

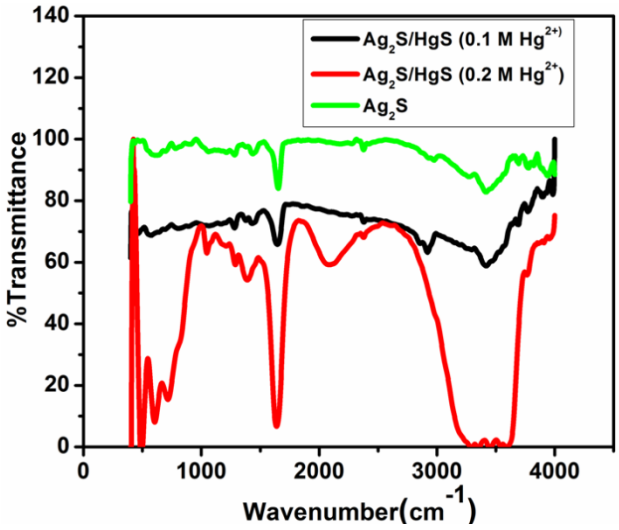

Fig. 2.4 FTIR spectra of core Ag_2S and core-shell Ag_2S-HgS nanostructure

Fig. 2.4 represents the FTIR spectra for core Ag_2S and core-shell Ag_2S-HgS nanostructure. The green colored line indicates that of the pure Ag_2S nanostructure where the peak around1652 cm^{-1} corresponds to that of C=O stretching mode [32] which is visible in both core-shell nanostructures, only the transmittance intensity is found to be decreased than the core structure. In the core-shell structures one

additional peak is found which is around 500 cm^{-1} attributed to the formation of S-S bond in the core-shell structure [32]. The peak is more sharp in 0.2 M Hg^{2+} coated Ag_2S sample. The peak around 3500 cm^{-1} corresponds to O-H stretching mode in the sample which is broadened in case of 0.2 M $HgCl_2$ coated Ag_2S nanostructures [30-32].This broadening occurs due to defects formed at the interface of the core-shell structure as a result of lattice mismatch between core and shell.

2.3 Optical Property Analysis

2.3.1 UV-Vis Absorbance spectra analysis

The absorption spectra of the samples are monitored with the help of a Shimadzu 2450 UV-vis spectrophotometer in the wavelength range from 200-900 nm with a deuterium source for scanning the UV range and a tungsten source for scanning the visible region. The basic unit of the spectrophotometer includes a source (UV and visible), a monochromator, sample container, detector, signal processor and a read out device [23-24]. The monochromator comprises of an entrance slit, a collimator that renders the light beam parallel, a prism or grating for dispersing the radiation beam, a focusing lens and an exit slit to isolate the desired spectral band from other dispersed radiation [23-24]. The detector converts the electromagnetic radiation into an electron flow thereby to a current or voltage flow in the readout circuit [23]. The absorption coefficient, α, due to interband transition near the band-gap is well described by the relation $\alpha\hbar\omega = B\,(\hbar\omega - E_g)^n$, where n=1/2 for indirect band gap semiconductor and 2 for direct band gap. $\hbar\omega$ is photon energy, E_g is optical gap. This Tauc plot defines the optical gap in amorphous semiconductors.

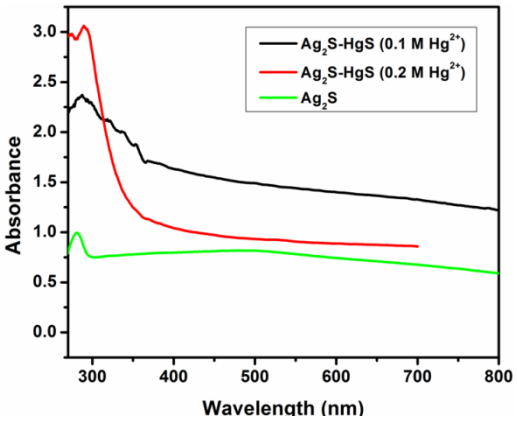

Fig. 2.5: UV-Vis absorption spectra

Fig. 2.5 shows the UV-Vis absorbance spectra for both core and core-shell nanostructures as indicated in the diagram, the green colored line represents the absorbance spectra of core Ag_2S nanostructure with a sharp peak around 280 nm. The long tail indicates inhomogeneous size distribution in the sample [25]. From, the red colored line (Ag_2S/ 0.1 M Hg^{2+}),it is found that there is slight red shift in the absorbance spectra where the peak is around 284 nm and a broadened one than the earlier one [26]. For the black colored spectra (Ag_2S /0.2 M Hg^{2+}), peak is found at 290 nm. The shifting in the absorbance peaks indicates increase in size of the sample gradually.

2.3.2 Photoluminescence spectra analysis

Photoluminescence (PL) spectroscopy is a complimentary technique to UV-vis absorption spectroscopy which measures the amount of light radiated by the material on excitation at a particular wavelength. This is a sensitive method to realize the discrete electronic states, surface and interface impurity levels and the quality of a material [27-28]. A steady state photoluminescence spectrometer is built with a continuous light source for exciting the material and a collimating lens for collecting the light. The light passes through a monochromator is collected into a photon detector or photomultiplier tube (PMT). The output signal is routed to a lock in amplifier. The steady state spectroscopy as well as time resolved photoluminescence spectroscopy can provide much valuable information on the lifetime of carriers.

Fig 2.6 depicts the photoluminescence spectra of core Ag_2S nanostructures and core-shell Ag_2S-HgS nanostructures (with 0.1 M Hg^{2+} and 0.2 M Hg^{2+}). The black colored line corresponds to the emission spectra of core Ag_2S nanostructures with a sharp band edge emission peak around 375 nm. From the picture, it is observed that the intensity of the band edge emission peak in core Ag_2S NC is enhanced about 7 times in the core-shell Ag_2S-HgS nanostructure (with 0.1 M Hg^{2+}) with the occurrence of a new peak surrounding 575 nm attributed to the formation of shell layer of HgS around it. When we further increase the Hg^{2+} concentration in the sample, it is discovered that the band edge emission peak is suppressed than in the core structure, but the intensity of the peak due to the shell component is found to be enhanced than the previous case and also red shifted indicating that there is an increase in shell thickness. This

demonstrates a transition from TYPE 1 to TYPE 2 core-shell nanostructure with increasing thickness of shell in the sample. The transition of TYPE 1 to TYPE 2 structure in the sample is further confirmed from the calculation of band gap for each sample

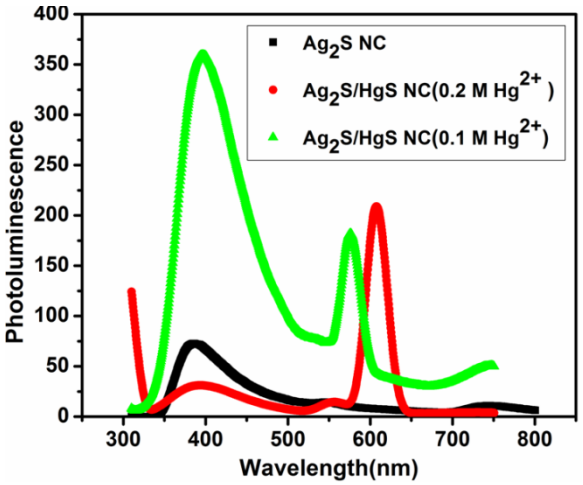

Fig. 2.6: Room temperature PL spectra of core Ag_2S nanostructures and core-shell Ag_2S-HgS nanostructures (with 0.1 M Hg^{2+} and 0.2 M Hg^{2+}) (λ_{ex}=350 nm)

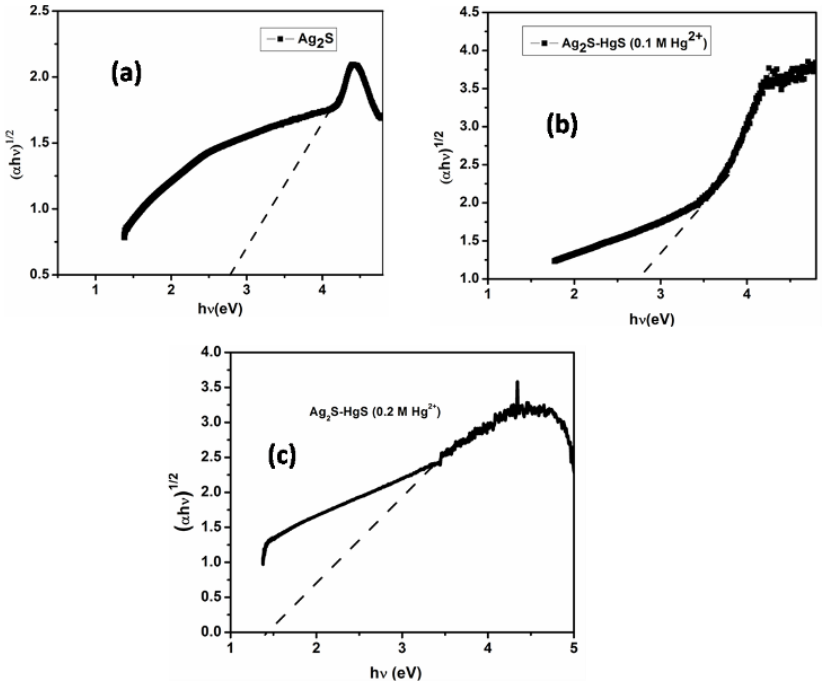

Fig. 2.7: Tauc's Plot (a) Ag_2S nanoparticles (b) Core-shell Ag_2S-HgS nanostructure (with 0.1 M Hg^{2+}) (c) Core-shell Ag_2S-HgS nanostructure (with 0.2 M Hg^{2+})

The band gap of the samples are calculated with the help of Tauc's plot from the absorbance spectra by using the following equation [29]

$$(h\nu\alpha)^{1/2}=A(h\nu-E_g)\text{……..(4)}$$

Where h=Planck's constant, ν=frequency of the incident light, α=Absorption coefficient, A=Proportionality constant, E_g= Band gap.

So by plotting hν along X-axis and $(h\nu\alpha)^{1/2}$ along Y-axis and taking the intercept of the linear section of the graph, the band gaps are calculated [34].

From the above Fig. 2.7, the band gaps are calculated as E_{Ag2S}= 2.75 eV, $E_{Ag2S\text{-}HgS}$ (0.1 M Hg^{2+})= 2.75 eV and $E_{Ag2S\text{-}HgS}$ (0.2 M Hg^{2+})=1.25 eV, where E corresponds to band gap for each sample. From the above parameters, it is found that E_{Ag2S}=$E_{Ag2S/HgS}$ (0.1 M Hg^{2+}) > $E_{Ag2S/HgS}$ (0.2 M Hg^{2+}). It has already been established that if Ecore=Ecore-shell, it represents TYPE 1 core-shell nanostructure whilst if Ecore-shell<Ecore it represents TYPE 2 core-shell nanostructure [7]

This implies that there is a transition of TYPE 1 to TYPE 2 core-shell nanostructure with increasing shell thickness and is further explained with the help of fig. 2.8 which is derived from a theoretical model proposed by Sergei .A. Evanov and his co-workers [7]. The transition from TYPE 1 to TYPE 2 is also established with the help of strain calculation which is discussed earlier.

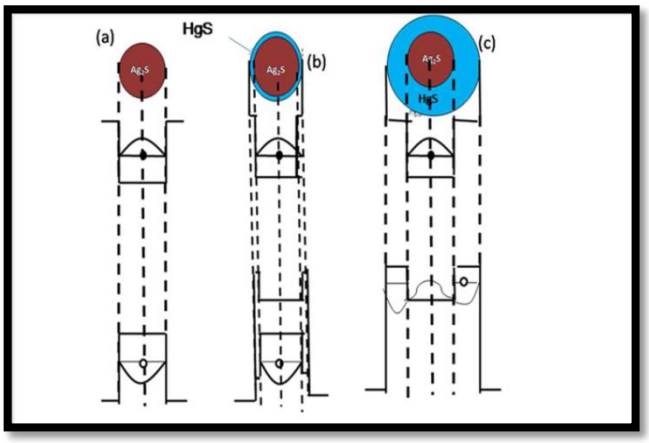

Fig. 2.8: Different localization regimes of core-shell Ag_2S-HgS with varying shell thickness (a) Ag_2S nanoparticles (shell thickness=0) (b) Core-shell Ag_2S-HgS (0.1 M Hg^2+) (shell thickness very small) (c) Core-shell Ag_2S-HgS (0.2 M Hg^{2+}) (shell thickness large)[7]

In Fig. 2.8, the left side picture depicts the carrier localization in case of the core Ag_2S nanoparticles. Here, as we can see the electron is confined in the conduction band and the hole is locked in the valence band. The central picture where the shell thickness is very small shows the TYPE 1 core-shell nanostructure. Let us consider the radius of the core is $R>R_c$ which is the critical radius for localization for any electron in the core. In this case, the electron is locked in the core for any shell thickness. Since the shell thickness is very small $H<H_c$ which is the critical radius for localization for any hole in the shell, so the hole is locked up in the valence band of the core regime only [7]. The image in the right side shows TYPE 2 core-shell nanostructure where the electron resides in the core regime but since the hole thickness $H>H_c$, so the hole tends to localize in the shell region. As we can see in case of TYPE 1 core-shell nanostructure, there is an overlap between the electron and hole hence the probability of recombination increases as a result there is a tremendous increase in photoluminescence of the sample. But in TYPE 2 core-shell nanostructures, the electron-hole overlap integral is almost equal to zero, so there is very less probability of recombination in the sample as a result the quantum yield efficiency decreases as we found in the photoluminescence spectra [7].

2.3.3 Photocatalytic activity study

Photocatalytic activities of pure Ag_2S nanoparticles and core-shell Ag_2S-HgS nanoparticles are studied by monitoring the degradation of phenol and methylene blue (MB) under daylight. The photoactivity is observed under daylight lamp of 500 watt power Xenon lamp in the wavelength range from 400-700 nm. The samples are placed at 6 cm distance from the light in the photocatalysis chamber. For carrying out the degradation experiment, 50 mg of the catalyst is added to 50 mL of methylene blue solution in a 100 mL beaker, with an initial methylene blue concentration of 10 mgL^{-1}. The solution is stirred in dark for 45 min for adsorption-desorption equilibrium. The catalyst loaded dye solution is irradiated under daylight for different time limits. When irradiation process is completed, each of the solution is centrifuged at 10,000 rpm to make it free from the catalyst. 5 mL of each of the irradiated methylene blue solution is taken for absorption measurement.

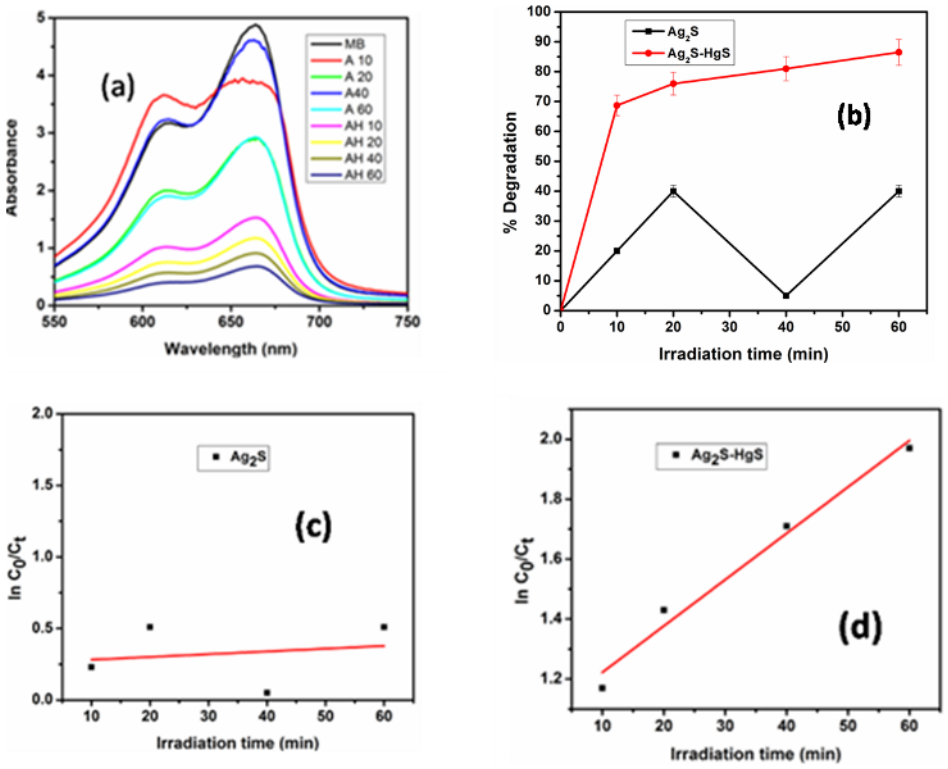

Fig 2.9: (a) Absorbance of MB in presence of catalyst (b) % Degradation vs time and rate constant determination of (c) Ag_2S (d) Ag_2S-HgS

The decrease of concentration or degradation of methylene blue from its initial concentration is studied by observing the decrease of the absorption peak (C_t) of the dye solution irradiated for the aforementioned period. The degradation efficiency of phenol solution is given by $\{(C_0-C_t)/C_0\}\times100\%$ [33]. The photocatalytic degradation process is expected to follow 1st order kinetics which follows the equation [35].

$$\ln Co/C_t - Kt = 0 \ldots\ldots\ldots\ldots\ldots\ldots\ldots\ldots$$

Where K is the rate constant. So by plotting $\ln C_o/C_t$ vs time and then taking the slope we can get the value of rate constant K.

Table 2.2: Rate constant determination and degradation efficiency

Sample name	Rate const (min^{-1})	% degradation w.r.t time of irradiation			
		10 min	20 min	40 min	60 min
Ag_2S	0.00487	20	40	5	40
Ag_2S-HgS	0.027	68.7	76	81	86.5

From the table 2.2, we can see that pure Ag_2S nanoparticles have shown a maximum degradation efficiency of 40% in both 20 min and 60 min irradiation of daylight. Basically Ag_2S nanomaterials can be a potential photocatalytic agent under sunlight as the bulk band gap which is 1.1 eV covers the entire solar spectrum for absorbance. But when we reduced the size to nano, as we have found from UV-vis absorbance spectra, the optical band gap is estimated to be 3.1 eV which mainly falls in the UV regime. Still, there is an extended absorbance tail upto 900 nm because of which we are able to get may it be little but some amount of photo degradation. We chose Ag_2S-HgS (0.2 M Hg^{2+}) to test photocatalytic activity and it has proved as an excellent photocatalyst by degrading the dye upto 86% under 60 min illumination. This is because, as stated earlier, the band gap of this sample comes near 1.2 eV which is once again very much suitable for solar catalysis due to wide range of absorbance. Even from the absorbance spectra, we can see a clear hump around 900 nm indicating the extended absorbance region. Another important criteria for photocatalysis is charge separation which we already established in case of Ag_2S-HgS (0.2 M Hg^{2+}). Since with increasing shell thickness, it attains a TYPE 2 configuration, charge separation becomes very much prominent in the sample which allows the free electrons and holes to move to the surface of the material where the dye is adsorbed and thus take part in photocatalytic reaction. We found that with increasing irradiation time, the degradation efficiency is also increasing owing to more photogeneration of charge carriers.

2.4 Conclusion

Thus we have successfully synthesized both Ag_2S nanoparticles and core-shell Ag_2S-HgS nanostructure via a simple chemical method. The structural properties are studied with the help of XRD and EDX spectra which reveals the presence of both core and shell in the sample and the morphological properties are studied with the help of

HRTEM. On studying the spectroscopic properties, a transition from TYPE 1 to TYPE 2 is found in the nanostructure with increasing shell thickness which is in accordance with the theory. No quasi TYPE 2 structure was observed while changing the shell concentration in the core-shell structure. Since in case of TYPE 2 core-shell nanostructures, the recombination probability is very low as suggested by the photoluminescence analysis, they are very much suitable material for photovoltaic, photo catalysis etc. When tested for photocatalytic activity, the TYPE 2 core-shell structure showed impressive degradation efficiency under daylight illumination.

References

[1] Lu, X., et al. Preparation and characterization of Ag_2S nanoparticles embedded in polymer fibre matrices by electrospinning, *Nanotechnology* **16**, 2233--2237, 2005.

[2] Dutta, D., & Ghosh, A. Role of Ag_2S Nanoparticles on the Dynamics of Silver Ions in Silver−Ultraphosphate Glass Nanocomposites, *J. Phys. Chem. C.* **113**, 9040--9046, 2009.

[3] Kryukov, A.I., et al. Optical and catalytic properties of Ag_2S nanoparticles, *J. Mol. Catal. A: Chem.* **221**, 209--221, 2004.

[4] Liu, S. H., et al. Synthesis and Characterization of Ag_2S Nanocrystals in Hyperbranched Polyurethane at Room Temperature, *J. Solid State Chem.* **168**, 259--262**,** 2002.

[5] Pan, H., et al. Aminopolycarboxyl-modified Ag_2S nanoparticles: Synthesis, characterization and resonance light scattering sensing for bovine serum albumin, *Talanta* **71**, 276--281, 2007.

[6] Günter Schmid, Nanoparticles: From Theory to Application, Germany, 2004.

[7] Evanov, S.A., et al. Type-II Core/Shell CdS/ZnSe Nanocrystals: Synthesis, Electronic Structures, and Spectroscopic Properties, *J. Am. Chem. Soc.* **129**, 11708--11719, 2007.

[8] Balet,L., et al. Inverted Core/Shell Nanocrystals Continuously Tunable between Type-I and Type-II Localization Regimes, *Nanoletters* **4**, 1485--1488, 2004.

[9] Qian, X. F., et al. Preparation and characterization of polyvinylpyrrolidone films containing silver sulfide nanoparticles, *J. Mater. Chem.* **11**, 2504--2506, 2001.

[10] Hiisselbartb, A., et al. Chemistry and photophysics of mixed cadmium sulfide/mercury sulfide colloids, *J. Phys. Chem.***97**, 5333--5340, 1993.

[11] Cullity, B.D. *Elements of X-ray diffraction*, Prentice Hall, New Jersey, 2001.

[12] Borchert, H., et al. Determination of nanocrystal Sizes: A comparison of TEM, SAXS, and XRD studies of highly monodisperse $CoPt_3$ Particles, *Langmuir* **21** (5), 1931--1936, 2005.

[13] Petkov, V., et al. Atomic-scale structure of nanocrystals by high-energy X-ray diffraction and atomic pair distribution function analysis: Study of Fex Pd_{100-x} (x =0, 26, 28, 48) Nanoparticles, *J. Phys. Chem. C*. **111** (2), 714--720, 2007.

[14] Gubicza, J., et al. Crystallite-size distribution and dislocation structure in nanocrystalline HfNi5 determined by X-Ray diffraction profile analysis, *J. Nanosci. Nanotechnolog.* **1**(3), 343--348, 2001.

[15] Onwudiwe, D.C., & Ajibade, P.A. ZnS, CdS and HgS Nanoparticles via Alkyl-Phenyl Dithiocarbamate Complexes as Single Source Precursors, *Int. J. Mol .Sci.* **12**, 5538--5551, 2011.

[16] Shenyuan, Y., et al. Strain-Induced Band Gap Modification in Coherent Core/Shell Nanostructures, *Nano Lett.* **10**, 3156--3162, 2010.

[17] Smith, A. M. et al. Tuning the Optical and Electronic Properties of Colloidal Nanocrystals by Lattice Strain, *Nat. Nanotechnol.* **4**(1), 56--63, 2009.

[18] Egerton, R.F. Physical Principles of Electron Microscopy: An Introduction to TEM, SEM, and AEM, Springer, New York, 2005.

[19] Williams, D.B., & Carter, B.C. Transmission Electron Microscopy,A Textbook for Materials Science, Springer, New York, 2009.

[20] Kaufmann, E.N. (ed.). *Characterization of Materials*, John Willey & Sons, New Jersey, 2003.

[21] Reed, A.J. G. & Bell, D.C. *Energy Dispersive and X-Ray Analysis in the Electron Microscope,* BIOS Scientific Publishers Limited, Oxford, 2003.

[22] http://serc.carleton.edu/research-education/geochemsheets/eds.html

[23] Lin, Y.B., et al. Ferromagnetism of Co-doped TiO_2 films prepared by plasma enhanced chemical vapour deposition (PECVD) method, *J. Phys. D: Appl. Phys.* **41** (19), 195007, 2008.

[24] Choudhury, B., et al. Effect of oxygen vacancy and dopant concentration on the magnetic properties of high spin Co^{2+} doped TiO_2 nanoparticles, *J. Magn. Magn. Mater*. **323** (5), 440--446, 2011.

[25]Yu, B., et al. Exciton spectra of SnO_2 nanocrystals with surficial dipole layer, *Optical Materials* **7**, 15--20, 1997.

[26] Sadowski, M. L., et al. Optical Properties of Semiconductor Nanostructures, The Netherlands, 2000, pp.389.

[27] Li, J.G., et al. Phase Structure and Luminescence Properties of Eu^{3+}-Doped TiO_2 Nanocrystals Synthesized by Ar/O_2 Radio Frequency Thermal Plasma Oxidation of Liquid Precursor Mists, *J. Phys. Chem. B.* **110** (3), 1121--1127, 2006.

[28] Wu, Q., et al. Creating oxygen vacancies as a novel strategy to form tetrahedrally coordinated Ti^{4+} in Fe/TiO_2 Nanoparticles, *J. Phys. Chem. C*. **116** (12), 7219--7226, 2012.

[29] http://en.wikipedia.org/wiki/Tauc_plot last accessed on 29/02/12

[30] http://mmrc.caltech.edu/FTIR/FTIRintro.pdf last accessed on 03/03/12

[31] http://www.daham.org/basil/leedswww/ftir/ftir_principle.htm last accessed on 03/03/12

[32]http://www2.chemistry.msu.edu/faculty/reusch/VirtTxtJml/Spectrpy/InfraRed/infrared.htm last accessed on 29/02/12.

[33] Choudhury, B., et al. Extending Photocatalytic Activity of TiO_2 Nanoparticles to Visible Region of Illumination by Doping of Cerium, *Photochemistry and Photobiology*, **88**, 257--264, 2012.

[34] Basyach. P. and Choudhury. A., Structural and optical properties of core–shell Ag_2S/HgS nanostructures, *Mater. Res. Bull.* **48**, 2543--2548, 2013.

[35] Seema, H., et al. Graphene–SnO2 composites for highly efficient photocatalytic degradation of methylene blue under sunlight, *Nanotechnology* **23**, 355705(1--8), 2012